Monthly Notices
of the
ROYAL ASTRONOMICAL SOCIETY

MNRAS **472,** 4587–4597 (2017)
Advance Access publication 2017 September 11

doi:10.1093/mnras/stx2349

Dust masses of $z > 5$ galaxies from SED fitting and ALMA upper limits

Hiroyuki Hirashita,[1⋆] Denis Burgarella[2] and Rychard J. Bouwens[3]

[1]*Institute of Astronomy and Astrophysics, Academia Sinica, PO Box 23-141, Taipei 10617, Taiwan*
[2]*Aix-Marseille Université, CNRS, LAM (Laboratoire d'Astrophysique de Marseille) UMR 7326, F-13388 Marseille, France*
[3]*Leiden Observatory, Leiden University, NL-2300 RA Leiden, the Netherlands*

Accepted 2017 September 7. Received 2017 September 6; in original form 2017 July 27

ABSTRACT

We aim at constraining the dust mass in high-z ($z \gtrsim 5$) galaxies using the upper limits obtained by Atacama Large Millimetre/submillimetre Array (ALMA) in combination with the rest-frame UV–optical spectral energy distributions (SEDs). For SED fitting, because of degeneracy between dust extinction and stellar age, we focus on two extremes: continuous star formation (Model A) and instantaneous star formation (Model B). We apply these models to Himiko (as a representative UV-bright object) and a composite SED of $z > 5$ Lyman break galaxies (LBGs). For Himiko, Model A requires a significant dust extinction, which leads to a high dust temperature >70 K for consistency with the ALMA upper limit. This high dust temperature puts a strong upper limit on the total dust mass $M_\mathrm{d} \lesssim 2 \times 10^6$ M$_\odot$, and the dust mass produced per supernova (SN) $m_\mathrm{d,SN} \lesssim 0.1$ M$_\odot$. Such a low $m_\mathrm{d,\,SN}$ suggests significant loss of dust by reverse shock destruction or outflow, and implies that SNe are not the dominant source of dust at high z. Model B allows $M_\mathrm{d} \sim 2 \times 10^7$ M$_\odot$ and $m_\mathrm{d,SN} \sim 0.3$ M$_\odot$. We could distinguish between Models A and B if we observe Himiko at wavelength < 1.2 mm by ALMA. For the LBG sample, we obtain $M_\mathrm{d} \lesssim 2 \times 10^6$ M$_\odot$ for a typical LBG at $z > 5$, but this only puts an upper limit for $m_\mathrm{d,SN}$ as $\sim$2 M$_\odot$. This clarifies the importance of observing UV-bright objects (like Himiko) to constrain the dust production by SNe.

Key words: dust, extinction – galaxies: evolution – galaxies: high-redshift – galaxies: ISM – galaxies: star formation – submillimetre: galaxies.

1 INTRODUCTION

Dust plays an important role in the evolution of galaxies and their interstellar medium (ISM). Dust surfaces are the main site for the formation of some molecular species, especially H_2 (e.g. Gould & Salpeter 1963; Cazaux & Tielens 2004), inducing the formation of molecular clouds, which host star formation (e.g. Hirashita & Ferrara 2002; Yamasawa et al. 2011). In the later stage of star formation, dust cooling induces fragmentation (Omukai et al. 2005) and determines the typical stellar mass (Schneider et al. 2006).

Dust also modifies the appearance of galaxies by absorbing and scattering stellar light and re-emitting it into far-infrared (FIR)[1] wavelengths. Therefore, dust dramatically modifies the observed spectral energy distributions (SEDs) of galaxies (e.g. Takeuchi et al. 2005). From a theoretical point of view, consistent modelling of dust extinction (dust absorption and scattering) and dust re-emission is crucial to understand and constrain the dust properties robustly (e.g. Calzetti 2001; Buat et al. 2012). In other words, modelling only one of dust extinction and dust emission is a highly degenerate problem as mentioned below. Precisely speaking, we should refer to the difference between the intrinsic stellar SED and the observed SED as dust attenuation (not dust extinction), since complex effects of radiation transfer in the galaxy also matters (Calzetti 2001; Inoue 2005). However, because there is no risk of confusion in this paper, we simply use the term 'extinction' without strictly distinguishing between extinction and attenuation.

Dust extinction could be estimated to match the SED at ultraviolet (UV) and optical wavelengths with a given stellar intrinsic SED. However, it is generally difficult to separate the effect of dust extinction and that of stellar age, since both effects make the SED red. Moreover, the SED also depends on the shape of extinction curve (i.e. the wavelength dependence of dust extinction). Therefore, without any assumption on the intrinsic stellar SED and extinction curve shape, determining the age and extinction is a highly degenerate problem.

This degeneracy could be resolved at least partially if we additionally use the FIR dust emission. Because the stellar radiation energy absorbed by dust is emitted in the FIR, the total FIR emission constrains the total dust extinction. Indeed, this energy balance between dust absorption and emission has been used to derive the total dust extinction (Buat & Xu 1996; Buat & Burgarella 1998;

⋆ E-mail: hirashita@asiaa.sinica.edu.tw

[1] In this paper, we simply use the term FIR for the wavelength range where the emission is dominated by dust.

Takagi, Arimoto & Vansevičius 1999). Therefore, this energy balance is the key to understand the effect of dust extinction on the SED shape ranging from UV to FIR.

The link between UV extinction and FIR emission has been investigated with the so-called IRX–β relation, where the IRX is the infrared excess (FIR-to-UV flux ratio) and β is the UV slope. This relation indicates that a large dust extinction leads to a red UV SED and a high IRX (Meurer, Heckman & Calzetti 1999; Takeuchi et al. 2012). Although the IRX–β relation provides a powerful tool to investigate the dust extinction and emission properties in galaxies, we also observe a significantly different IRX–β relation at $z \gtrsim 5$ (z is the redshift) from the one at low redshift (Capak et al. 2015; Fudamoto et al. 2017). Different extinction curves as well as multiple dust temperature structures are possible reasons for the difference (Mancini et al. 2016; Bouwens et al. 2016, hereafter B16; Ferrara et al. 2017; Narayanan et al. 2017; Popping, Puglisi & Norman 2017). Because the IRX–β relation is not fully understood for high-z galaxies, it is still worth investigating the UV–FIR SED directly.

Recently, it has become possible to investigate the dust production and evolution in high-z galaxies.[2] To clarify the origin of dust in the Universe, it would be desirable to observe the first-generation galaxies, which is difficult at the current sensitivity of observational facilities. The most sensitive dust search at high z is possible by the Atacama Large Millimetre/submillimetre Array (ALMA). The highest z galaxies for which the dust emission is detected by ALMA are located at $z > 7$ (Watson et al. 2015; Willott et al. 2015; Laporte et al. 2017). The high sensitivity of ALMA enables us to constrain the dust enrichment processes in those galaxies (Mancini et al. 2015; Wang, Hirashita & Hou 2017). However, dust continuum has not been detected for most Lyman break galaxies (LBGs) at $z \gtrsim 6$ (Aravena et al. 2016; B16).

Ouchi et al. (2013, hereafter O13) observed a Lyman α (Lyα)-emitting gas blob 'Himiko' at $z = 6.6$ using ALMA. O13 put an upper limit of 0.0521 mJy (3σ) at 1.2 mm for Himiko. Hirashita et al. (2014, hereafter H14) developed a method to constrain the dust mass formed per supernova (SN) based on O13's result. They basically divided the total dust mass by the total number of SNe estimated from the UV luminosity, taking into account the fraction of dust destroyed by SN shocks sweeping the ISM (see also Michałowski 2015). They obtained an upper limit of dust mass formed per SN for Himiko as $\sim$0.15–0.45 $M_\odot$ depending on the assumed grain species. The obtained dust mass indicates that a significant fraction of the dust once condensed in an SN is destroyed in the shocked region before being injected into the ISM. This destruction is referred to as reverse shock destruction.

The above analysis in H14 treated the UV and FIR SEDs separately. As explained above, the SEDs in those two wavelength ranges are tightly related through dust absorption and re-emission. It would be interesting to re-examine the above constraint on the SN dust production by treating those two wavelength ranges consistently with a single SED model. Therefore, in this paper, we apply an SED model to the observed SED of Himiko and re-examine the constraint on the dust mass. The advantage of using such an SED argument is that we guarantee the energy balance between absorption and re-emission.

Although most LBGs at $z \gtrsim 6$ are not detected by ALMA, we expect that we could obtain a stringent upper limit for the dust emission of a typical LBG by stacking all the non-detections. Therefore, another purpose of this paper is to constrain the dust mass for high-z LBGs. Because the number of high-z LBGs observed by ALMA is expected to increase, the method developed here could also be applied to a larger sample in the future. Because only a small number of LBGs are detected by ALMA, we concentrate on the non-detections for the uniformity of the sample. Detailed analysis of detected high-z objects is given in our separate paper (Burgarella et al., in preparation).

There are a large number of SED models based on stellar population synthesis and dust attenuation treatment (Conroy 2013, for a review). Some of them solve radiation transfer in a dusty ISM to obtain the SED (e.g. Silva et al. 1998; Takagi, Vansevicius & Arimoto 2003; Bianchi 2008; Baes et al. 2011; Popescu et al. 2011; De Looze et al. 2014; Yajima et al. 2014). Although radiation transfer modelling enables us to take realistic spatial distributions of dust and stars into account, it generally has a high computational cost. Moreover, little is known about the geometry of dust and stellar distributions for high-z galaxies, which means that apparent morphologies cannot be used to constrain the model. Given the situation, a simple SED model that is computationally less expensive but still considers the energy balance between dust extinction and emission is useful for high-z galaxies. In this case, instead of solving radiation transfer, we treat the galaxy as a single-zone object, but we are able to run a lot of cases for different dust extinctions, dust properties (especially, extinction curves) and stellar population ages. There are some SED models suitable for such a purpose (Burgarella, Buat & Iglesias-Páramo 2005; da Cunha, Charlot & Elbaz 2008). The basic idea of these models is that the stellar light is synthesized based on the star formation history, attenuated according to the assumed dust extinction curve, and re-emitted in the FIR. Among them, we adopt CIGALE (Noll et al. 2009), but the results in this paper will not be changed even if we adopt other SED models.

This paper is organized as follows. In Section 2, we explain the observational data and the SED model. In Section 3, we show the results of the SED fitting and dust mass estimates. In Section 4.1, we constrain the dust production rate by SNe based on the results. In Section 5, we discuss the limitation of our method and the implication of our results for dust enrichment at high z. In Section 6, we give the conclusion of this paper. We use $(h,\ \Omega_\mathrm{m},\ \Omega_\Lambda) = (0.7,\ 0.3,\ 0.7)$ for the cosmological parameters.

2 SED FITTING

2.1 Data

For the direct comparison with H14, we adopt Himiko (a large Lyα emitting galaxy) to constrain the dust mass. Since Himiko is one of the brightest galaxies in the rest UV at $z > 6$ but is not detected by ALMA, it has potentially very low FIR-to-UV luminosity ratio. This leads to a stringent limit for the dust production in the early epoch of galaxy evolution. We adopt the rest-frame UV–optical SED data in O13 for Himiko.

Other than Himiko, there have been a lot of high-z galaxies, mainly LBGs, observed by ALMA. One of the largest samples can be found in B16. None of the sample LBGs at $z > 5$ in B16 was detected by ALMA. Although each LBG gives only a weak constraint on the dust production compared with Himiko, stacking the large sample could enable us to obtain a strong constraint on the dust mass. In fact, a small number of LBGs are detected by ALMA at $z > 5$ (Capak et al. 2015; Watson et al. 2015; Laporte et al. 2017). Since these galaxies need SED fitting and detailed analysis one by one, we treat them in our future paper (Burgarella

[2] In this paper, we refer to $z > 5$ as high redshift.

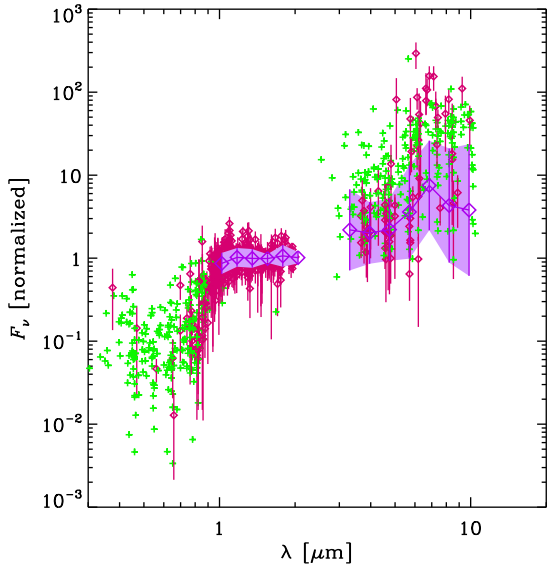

Figure 1. SEDs of the B16 LBG sample shifted to $z = 6.6$ and normalized to the flux at rest 0.2 μm (i.e. 1.52 μm in this figure). The wavelength in this figure (and also in the following figures) is shown in the observer's frame. The small squares with error bars show detected data points while the crosses show upper limits. The large squares show the composite SED with the shaded regions corresponding to the dispersion for the data at $\lambda < 3$ μm and to the upper and lower ranges for the data at $\lambda > 3$ μm (see the text for details). The normalization of the composite SED at 1.52 μm is determined as 9.3 nJy.

et al., in preparation). We emphasize that a major part of LBGs are not detected by ALMA and that they can be analysed uniformly with our method developed in this paper. The methodology established here could be applied to any future larger sample. For the first step, we produce a composite (or stacked) SED for the B16 sample.

We select galaxies at $z \geq 5.0$ in B16 (78 objects in total). The redshift of the sample extends up to $z = 9.8$, and most of the samples are located at $z < 7$ with 13 exceeding $z = 7$. First of all, we need to make the redshifts uniform. In principle, we can choose any redshift; however, for this paper, it is convenient to choose Himiko's redshift ($z = 6.6$) since we can utilize the same SED models. For an LBG at original redshift $z_{\rm orig}$, we move it virtually to $z = 6.6$ by shifting the wavelength by $\lambda(1 + z)/(1 + z_{\rm orig})$ and multiplying the flux with $[(1 + z)/(1 + z_{\rm orig})][d_{\rm L}(z_{\rm orig})/d_{\rm L}(z)]^2$, where $d_{\rm L}(z)$ is the luminosity distance at redshift z (Carroll, Press & Turner 1992).

Next, since the flux level is diverse among the sample LBGs, we need to normalize the SED at a certain wavelength, in order to extract the information on the SED shape. For this purpose, we normalize the flux to the value at rest 0.2 μm (i.e. 1.52 μm after shifting the SED). The flux at rest 0.2 μm is estimated from the flux at the two nearest wavelengths by interpolation or extrapolation and divide the fluxes at all the sampled wavelength by the 0.2-μm flux. The shifted and normalized fluxes for all the samples are plotted in Fig. 1.

Based on the above normalized SEDs of the sample, we make a composite SED. As we observe in Fig. 1, the SEDs are roughly divided into the three parts: at $\lambda < 0.92$ μm, most of the points are upper limits because the radiation is absorbed by hydrogen atoms in the interstellar or intergalactic medium on the line of sight. We do not use the data in this wavelength range for the fitting below. At $0.92 < \lambda < 3$ μm, most of the points are detected data; thus, we neglect the data without detection in this wavelength range. We divide the data into six bins with a logarithmically equal width (0.95–1.09, 1.09–1.26, 1.26–1.44, 1.44–1.66, 1.66–1.91 and 1.91–2.20 μm). We take the average of the logarithmic values of the normalized data points in each bin to obtain the composite SED. We also estimate the logarithmic dispersion as shown in Fig. 1. At $\lambda > 3$ μm, a large fraction of the data points are not detected. In this wavelength range, thus, we would overestimate the averaged flux if we neglect all the points without detection. To avoid such an overestimate, we derive the probable range of the composite SED at $\lambda > 3$ μm by estimating upper and lower bounds in the following way. First, we set seven bins with a logarithmically equal width (3.00–3.60, 3.60–4.32, 4.32–5.18, 5.18–6.22, 6.22–7.46, 7.46–8.96 and 8.96–10.7 μm). We average the logarithmic upper and lower bounds of the sample to obtain the upper and lower limits, respectively, in each wavelength bin. For detected data points, we simply use the observed flux for both upper and lower bounds. For non-detections, we use the upper limit given by B16, while we give a lower limit by adopting the value estimated from the bluest SED as explained below. The bluest SED under a fixed $\lambda = 1.52$ μm (rest 0.2 μm) flux gives the lowest possible flux at $\lambda > 3$ μm, and can be estimated by extrapolating the rest 0.2 μm flux (i.e. unity after the normalization) with a power-law $f_\nu \propto \lambda^{\beta_{\rm UV}+2}$, where $\beta_{\rm UV}$ is the spectral slope at rest UV wavelengths (Calzetti, Kinney & Storchi-Bergmann 1994). If we adopt the smallest possible value of $\beta_{\rm UV}$, we obtain a lower limit of the flux. The smallest value of $\beta_{\rm UV}$ is determined by the intrinsic stellar UV SED; thus, we adopt $\beta_{\rm UV} = -2.5$ (Bouwens et al. 2014). For the fitting, we allow for the full range between the upper and lower limits and adopt the logarithmic average of these two limits as the representative value in each wavelength bin. Finally, the normalized flux is multiplied by the logarithmically averaged rest 0.2 μm flux (9.3 nJy) to obtain the absolute level of the flux.

The upper limits of the 1.2 mm flux given by B16 are utilized to obtain the upper limit of the millimetre (mm) flux for the composite (or stacked) SED. First, we obtain a stacked upper limit by $\bar{f}_{\rm mm} = \sqrt{\sum_i \sigma_i^2}/N$, where σ_i is the 1σ noise level for the ith galaxy. Next, we calculate the mean redshift $\bar{z} = 6.1$ for the B16 sample. The wavelength (1.24 mm) and the upper limit flux $\bar{f}_{\rm mm}$ are shifted in the same way as above to obtain the corresponding values at $z = 6.6$. Consequently, we obtain a 3σ upper limit value of 6.7 μJy at 1.31 mm.

2.2 SED code – CIGALE

We use CIGALE (Code Investigating GALaxy Emission; Noll et al. 2009) to produce the UV–submm SED of a galaxy. It takes into account the energy balance between the stellar light extinguished by dust and its re-emission in the FIR. The stellar population synthesis is based on Bruzual & Charlot (2003) and Maraston (2005). There are some freedoms in the parameter setting, which we set as described below.

We adopt a Chabrier initial mass function (IMF; Chabrier 2003), although applying a Salpeter IMF (Salpeter 1955) instead does not change our results below significantly. We also include emission lines, since they are known to contribute to the fluxes in some bands for star-forming galaxies. We use the following functional form for the star formation rate (SFR):

$$\mathrm{SFR}(t) = C(t/\tau_{\rm SF})\exp(-t/\tau_{\rm SF}), \quad (1)$$

where C (proportional to the total stellar mass, M_*) is the normalization constant adjusted in the fitting, t is the age, and $\tau_{\rm SF}$ is the star

formation time-scale. This functional form can mimic a continuous (or constant) SFR if we adopt a much longer $\tau_{\rm SF}$ than the age ($\tau_{\rm SF} \gg t$) while it represents a burst SFR if we take $\tau_{\rm SF} \ll t$.

For the dust SED, we adopt the CASEY2012 module, which is based on Casey (2012). In this SED model, the FIR emission is practically the so-called modified blackbody radiation that is described by a functional form of $\nu^{\beta} B_{\nu}(T_{\rm d})$, where ν is the frequency, $T_{\rm d}$ is the dust temperature and $B_{\nu}(T_{\rm d})$ is the Planck function. We are not interested in the power-law-like mid-infrared emission adopted in the CASEY2012 module in this paper. The advantage of this model is that we are able to give the dust temperature freely. We fix $\beta = 1.6$, but this choice does not affect the results below significantly as long as we adopt $\beta = 1$–2.

For the extinction law, we adopt the power-law form, since the detailed functional form is not important (and cannot be constrained) in this work. In this model, the extinction at wavelength λ is described by a given power-law index δ as

$$A_{\lambda} = A_V \left(\frac{\lambda}{0.55\,\mu{\rm m}} \right)^{\delta}, \tag{2}$$

where A_V is the extinction in the V band. We examine the following three cases for δ: $\delta \simeq -0.4$, -0.7 and -1.1, which roughly approximate a flat extinction curve as observed in a high-z quasar by Maiolino et al. (2004) and Gallerani et al. (2010), an attenuation curve representative of nearby starburst galaxies (Calzetti et al. 1994) and the Small Magellanic Cloud (SMC) extinction curve (Pei 1992), respectively. Note that the flat extinction curves in high-z quasars are also consistent with theoretically expected dust properties for SN dust production (Maiolino et al. 2004; Hirashita et al. 2005; Asano et al. 2014) or for strong grain growth by coagulation (Nozawa et al. 2015).

We also apply different extinctions (A_V) for the young ($<$10 Myr) and old ($>$10 Myr) stellar populations following Charlot & Fall (2000). We denote the extinction of the young population in the V band as A_V. We introduce a parameter $\eta \leq 1$ that expresses the extinction of the old population relative to that of the young population (i.e. the extinction of the old stellar population is ηA_V). According to Calzetti (2001), $\eta \simeq 0.44$ for nearby star-forming galaxies. We also examine other values such as $\eta = 0$ (no extinction for the stellar population with age $>$10 Myr) and $\eta = 0.9$ (almost no difference between the extinctions of stellar populations with different ages).

For each parameter set (A_V, $T_{\rm d}$, δ, η), we obtain an SED, and scale the total stellar mass (M_*) to minimize χ^2. The χ^2 is estimated using the logarithmic fluxes and errors (for the stacked LBG SED, we use the half width of the shaded range in Fig. 1 for σ at each wavelength bin). Although we do not use the ALMA upper limit for the fitting directly, we only accept the case in which the model flux at the ALMA band is below the 3σ upper limit. For Himiko, we choose the parameter sets of satisfactory fit based on a criterion of reduced $\chi^2 < 3$. We have confirmed that adopting more relaxed criterion as $\chi^2 < 5$ does not change the results below (in other words, the range of the acceptable parameter values does not become significantly wider). For LBGs, we also minimize χ^2 but only used the stacked data at $0.92\,\mu{\rm m} < \lambda < 3\,\mu{\rm m}$, and exclude the SEDs that are not within the dispersion shown in Fig. 1 in that wavelength range.

2.3 Extracting dust-related parameters

First, we performed fitting to the observed SED by freely varying relevant parameters in CIGALE. Overall, most of the parameters are not constrained mainly because of the well-known degeneracy between dust extinction and age, both of which contribute to the 'reddening' of the UV–optical SED. Only the age has a significant range of 440 ± 250 Myr, which is only weakly constrained though. Similar stellar ages are also obtained by O13. The stellar metallicity is not constrained; thus, we fix it to 0.004 ($\sim$1/5 $Z_{\odot}$) throughout this paper.

Considering the age–extinction degeneracy, we choose to focus on the two extreme (but still reasonable) cases: (A) blue stellar continuum with high extinction and (B) red stellar continuum with low extinction. These two cases are differentiated by the star formation time-scale $\tau_{\rm SF}$. For (A), we adopt $\tau_{\rm SF} = 2000$ Myr and $t = 400$ Myr. This case represents a gradually rising (SFR $\propto t/\tau_{\rm SF}$) star formation history up to the age $t = 400$ Myr (consistently with the above age constraint; note that the mean age of the stellar population is roughly 200 Myr in this case). This case is referred to as the continuous SFR. For (B), we adopt $\tau_{\rm SF} = 20$ Myr and $t = 200$ Myr. Since $\tau_{\rm SF} \ll t$, the mean stellar age is $\sim t = 200$ Myr, which is equal to the mean age of (A). This case is referred to as the burst SFR. The value of $\tau_{\rm SF}$ is chosen for the following reason. If $\tau_{\rm SF} \gtrsim 30$ Myr, the contribution from the young ($<$10 Myr) population is not negligible. In this case, the situation is similar to Model A and we need to include an appreciable amount of extinction. In contrast, $\tau \lesssim 10$ Myr is rejected since the intrinsic stellar SED is significantly redder than the observed SED of Himiko. Thus, we adopt $\tau = 20$ Myr to represent the case of red intrinsic stellar SED.

After fixing the star formation history, the remaining parameters that dominate the SED are those related to the extinction and emission of dust. Thus, the extinction A_V, which determines the energy emitted in the FIR, and $T_{\rm d}$, which regulates the peak wavelength of the FIR SED, are the most important parameters. As we will see later, further details of extinction also affect the results: in particular, δ and η regulate the SED colour in the UV–optical (smaller δ makes the stellar SED redder under a fixed A_V). As shown later, since δ and η show different effects on the stellar and dust SEDs, we vary both of those parameters.

In summary, we vary A_V, $T_{\rm d}$, δ and η in searching for a fitting solution. For δ and η, unless otherwise stated, we consider the following representative cases: $\delta = -0.4$, -0.7 and -1.1; $\eta = 0$, 0.44 and 0.9 (see Section 2.2). We move A_V and $T_{\rm d}$ (quasi) continuously. We basically apply the same procedure for both Himiko and the B16 LBG sample.

2.4 Constraint on the dust mass

The total FIR luminosity (=total stellar radiation energy extinguished by dust) and the dust temperature can be translated into the total dust mass. The flux density at frequency ν in the observer's frame can be written as (H14)

$$f_{\nu} = \frac{(1+z) \kappa_{(1+z)\nu} M_{\rm d} B_{(1+z)\nu}(T_{\rm d})}{d_{\rm L}^2}, \tag{3}$$

where κ_{ν} is the dust mass absorption coefficient at ν and $M_{\rm d}$ is the dust mass. H14 give the dust mass absorption coefficient at $\lambda = 158\,\mu{\rm m}$ (κ_{158}), which corresponds to the ALMA-observed wavelength at the redshift of Himiko ($z = 6.6$; 1.2 mm in the observer's frame). The mean wavelength of the B16 sample is 1.31 mm. The difference in the wavelength is corrected for κ_{ν} by assuming a dependence of $\kappa_{\nu} \propto \nu^{\beta}$ with $\beta = 1.6$ (i.e. consistent dependence with the SED fitting). Because this correction is small, the detailed wavelength dependence of κ_{ν} does not influence our results. We adopt the same dust species as in H14, and list the adopted values of κ_{ν} at 158 μm for each dust species in Table 1. Among

Table 1. Dust properties.

Species	$\kappa_{158}{}^{a}$ (cm^2 g^{-1})	$\kappa_{\rm sil}^{-1}{}^{b}$	Ref.^{c}
Graphite	20.9	0.63	1, 2
Silicate	13.2	1	1, 2
SN$^{d}_{\rm con}$	5.57	2.4	3
SN$^{e}_{\rm dest}$	8.94	1.5	4
AC^{f}	28.4	0.46	5, 6

Notes.[a]Mass absorption coefficient at 158 μm.
[b]Inverse of κ_{158} normalized to the silicate value. The dust mass obtained in this paper is basically for silicate; thus, if we multiply the dust mass with $\kappa_{\rm sil}^{-1}$, we obtain the dust mass for other dust species.
[c]References: (1) Draine & Lee (1984); (2) Dayal, Hirashita & Ferrara (2010); (3) Hirashita et al. (2005); (4) Hirashita et al. (2008); (5) Zubko et al. (1996); (6) Zubko, Dwek & Arendt (2004).
[d]Dust condensed in SNe before reverse shock destruction.
[e]Dust ejected from SNe after reverse shock destruction.
[f]Amorphous carbon.

the various dust species, silicate and graphite are used to model the extinction curves in nearby galaxies (Draine & Lee 1984; Pei 1992; Hou, Hirashita & Michałowski 2016). Since SNe may contribute to the quick dust enrichment in $z > 5$ galaxies (Todini & Ferrara 2001; Nozawa et al. 2003; Maiolino et al. 2004), we also use the mass absorption coefficient for the dust grains formed in SNe. We adopt the theoretically calculated mass absorption coefficient for dust condensed in SNe (SN$_{\rm con}$), which was obtained by Hirashita et al. (2005) using the dust species and grain size distribution in Nozawa et al. (2003). We also apply the dust properties after the so-called reverse shock destruction within the SN remnant (Nozawa et al. 2007; Hirashita et al. 2008, SN$_{\rm dest}$). In addition, we examine amorphous carbon (AC), which was used to model the SED of SN 1987A by Matsuura et al. (2011).

3 RESULTS

3.1 Himiko: Model A

For Model A ($\tau_{\rm SF} = 2000$ Myr and $t = 400$ Myr), because of the blue intrinsic stellar SED, dust extinction is strongly required. However, a large extinction also indicates a high dust FIR luminosity; in particular, Himiko has a very bright UV luminosity, which would lead to a high FIR luminosity even for a small amount of extinction. Because of the stringent upper limit at 1.2 mm, the smallest η and δ (i.e. $\eta = 0$ and $\delta = -1.1$) give the most relaxed condition for the extinction; that is, this choice of η and δ minimizes the FIR emission by restricting the extinction only to the youngest (<10 Myr) population and by reddening the UV SED most efficiently with the steepest extinction curve.

With $\eta = 0$ and $\delta = -1.1$, we find that the satisfactory fit solutions have the following properties. Only dust temperatures higher than ∼70 K are consistent with the ALMA upper limit. This is because, with a fixed FIR dust luminosity, the dust SED peak shifts to a shorter wavelength and the 1.2 mm flux becomes lower for a higher dust temperature. We also find a satisfactory fit for any value of

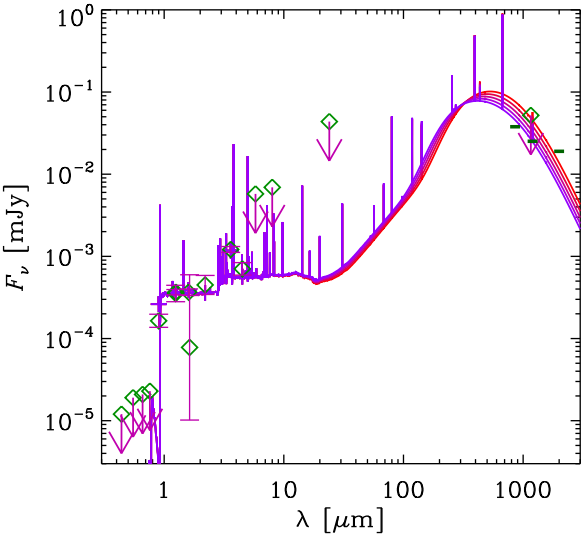

Figure 2. Examples of satisfactory fitting to the SED of Himiko in Model A. We adopt $A_V = 0.5$ mag, $\eta = 0$ and $\delta = -1.1$. The SEDs are shown for $T_{\rm d} = 70$, 75, 80, 85 and 90 K from the upper to lower lines at 1.2 mm. The data points (diamonds) are taken from O13. The data points with error bars show detected points, while those with arrows indicate upper limits. The short horizontal lines at 0.85, 1.2 and 2 mm show the 3σ detection limits for 5-h on-source integration by the full ALMA (50 12-m antennas).

$A_V \geq 0.5$ mag since the stellar SED is consistent with the sum of the populations with age > 10 Myr (recall that, with $\eta = 0$, we applied dust extinction only to stellar populations with age < 10 Myr). This means that it is important to extinguish the radiation from the youngest (<10 Myr) population. Thus, as examples of satisfactory fits, we show the cases of $A_V = 0.5$ mag, $\eta = 0$ and $\delta = -1.1$ with various dust temperatures in Fig. 2.

In Fig. 2, we also show the ALMA sensitivities expected for 5-h on-source integration with the full ALMA (50 12-m antennas) at wavelengths 0.85, 1.2 and 2 mm (frequencies 350, 250 and 150 GHz).[3] We observe that, because the required dust temperature is high, the SED falls steeply towards long wavelengths. As a consequence, a shorter wavelength band tends to detect Himiko more easily. It is expected that Himiko is detected at both 0.85 and 1.2 mm with the future full ALMA sensitivity, if Model A is appropriate for Himiko. Since the 0.85 mm band is near to the SED peak, detection at two wavelengths including 0.85 mm enables us to estimate the dust temperature and the total FIR luminosity under a given emissivity index (β). The total FIR luminosity constrains the total amount of dust extinction (i.e. A_V). The non-detection at ∼2 mm would also confirm a high dust temperature.

For a given set of (A_V, $T_{\rm d}$), we obtain the dust mass using the conversion from the predicted mm flux to the dust mass as described in Section 2.4. We adopt κ_ν of silicate. Note that the dust mass $M_{\rm d}$ is proportional to κ_ν^{-1}. For convenience, we list κ_ν normalized to the silicate value (denoted as $\kappa_{\rm sil}$) in Table 1, so that we can multiply the dust mass with $\kappa_{\rm sil}^{-1}$ to obtain the dust mass with a different dust species. In Fig. 3, we show the obtained dust mass corresponding to the set of (A_V, $T_{\rm d}$) by the grey-scale. We only show the dust mass in the area of (A_V, $T_{\rm d}$) where the fitting is satisfactory. The shaded regions show that the reduced χ^2 is larger than 3 or that the mm flux exceeds the ALMA upper limit. We obtain a lower dust mass for

[3] https://almascience.nao.ac.jp/proposing/sensitivity-calculator

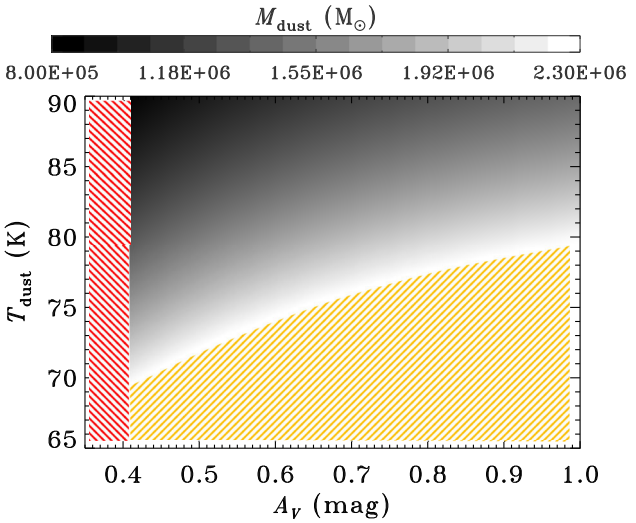

Figure 3. Dust mass derived from parameter set (A_V, $T_{\rm d}$) for Himiko in Model A. The dust mass corresponding to (A_V, $T_{\rm d}$) is shown by the grey-scale, and the level of dust mass is shown in the bar on the top. The dust mass is only shown in the area where the SED fitting is successful. The yellow shaded area is the region where the mm flux exceeds the ALMA upper limit, while the red shaded area is the region where we do not obtain a satisfactory fit to the rest UV–optical data (i.e. reduced $\chi^2 \geq 3$).

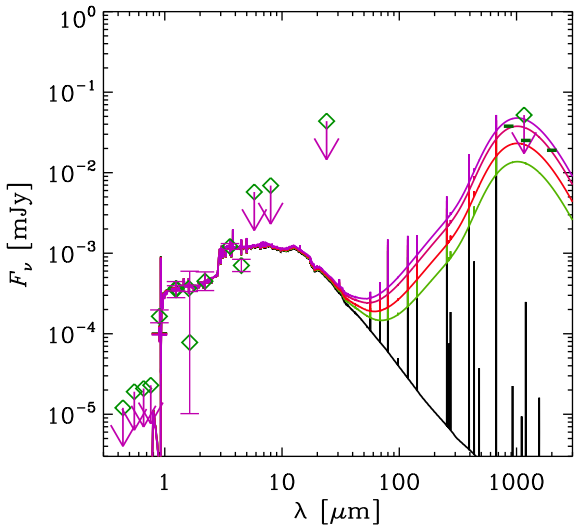

Figure 4. Examples of fitted SEDs for Himiko in Model B with $\eta = 1$, $T_{\rm d} = 30$ K and $\delta = -0.4$. The SEDs show the results with $A_V = 0$, 0.03, 0.05, 0.08 and 0.1 mag for the lower to upper lines at 1.2 mm. The data points and the short horizontal lines are the same as in Fig. 2.

a higher dust temperature partly because, as mentioned above (see Fig. 3), the 1.2 mm flux decreases with dust temperature under a fixed total FIR luminosity (i.e. under a fixed A_V) and partly because $B_\nu(T_{\rm d})$ is larger for higher $T_{\rm d}$ (see equation 3).

In Fig. 3, we observe that $A_V < 0.4$ mag is not allowed. This is because the rest UV–optical SED is too blue with small extinction. Moreover, the constraint on the dust temperature is not largely different among various values of A_V, because most of the UV radiation from the youngest stellar population is absorbed as long as $A_V \gtrsim 0.5$ mag; that is, the FIR luminosity is not sensitive to A_V if $A_V \gtrsim 0.5$ mag. Accordingly, the constraint on the dust temperature is only weakly dependent on A_V as long as $A_V \gtrsim 0.5$ mag. The lower limit for the dust temperature is 70 K at $A_V \sim 0.4$ mag and 80 K at $A_V \sim 1$ mag. The dust mass obtained is lower than 2.1×10^6 $M_\odot$. We use this value for the upper limit of the dust mass in Model A.

3.2 Himiko: Model B

We investigate Model B ($\tau_{\rm SF} = 20$ Myr and $t = 200$ Myr) for Himiko. In this case, the contribution from the stellar population younger than 10 Myr is negligible, so that the resulting SED is insensitive to η. Because ionizing photons are emitted by such a young stellar population (e.g. Kennicutt & Evans 2012), the strong Ly α emission observed for this galaxy may not be explained by recent star formation in this model. However, as discussed in Ouchi et al. (2009), there are mechanisms of Ly α emission other than recent star formation such as ionization by a hidden AGN, cooling of newly accreted gas, outflowing gas excited by shocks, etc. Therefore, Model B is still worth investigating, but we should keep in mind that the strong Ly α emission is not an indicator of the SFR in this case.

The intrinsic stellar SED is almost consistent with the observed SED in Model B; thus, extinction is not strongly required. Since the contribution from young stellar population is negligible, η is not important. Thus, we simply fix $\eta = 1$ (so A_V is the extinction for all stellar populations). We examine which set of (A_V, $T_{\rm d}$, δ) reproduces the observed SED with the same procedure as in Model A; that is, we extract the parameter sets that realizes reduced $\chi^2 < 3$ and the flux at 1.2 mm below the 3σ constraint of the ALMA observation. Below, we examine the area of (A_V, $T_{\rm d}$) that gives a good fit to the SED under a given δ (-0.4, -0.7 or -1.1).

As examples of satisfactory fitting, we show the SEDs with $\delta = -0.4$, $T_{\rm d} = 50$ K and various A_V in Fig. 4. For extinction, $A_V > 0.1$ mag is rejected because the UV–optical SED is too red to fit the observed SED. If we adopt a steeper extinction curve ($\delta = -0.7$ or -1.1), the constraint on A_V becomes more stringent since the UV–optical SED becomes redder with a smaller A_V.

Because A_V is strongly limited by the UV–optical SED in Model B, the FIR emission is consistent with the ALMA data point even if we adopt a low dust temperature such as $T_{\rm d} = 30$ K. In other words, the dust temperature is not constrained in this model. Therefore, $T_{\rm d}$ should be constrained by another method. H14 suggested that the dust temperature can be estimated by assuming radiative equilibrium between incident stellar radiation and dust FIR emission. The obtained equilibrium dust temperature is ~30 K; however, H14 argue that this is a lower limit because of the assumption that dust is distributed over the ALMA beam (in a radius of 2.2 kpc). In reality, it is expected that the dust is associated with the stellar distribution (or regions of recent star formation), which is more compact than the ALMA beam in Himiko (O13).

In fact, we cannot completely exclude a possibility that the dust temperature is lower than 30 K. In this case, the dust temperature is similar to the cosmic microwave background temperature, which is ~20.7 K at Himiko's redshift ($z = 6.6$). Ferrara et al. (2017) argue that high-pressure environment in high-z star-forming galaxies can accommodate dense regions where the dust is effectively shielded from the intense stellar radiation (see also Pallottini et al. 2017). Because the dust is 'dark' in this case, even ALMA may not be able to detect it.

In summary, Model B is reduced to a case of unconstrained dust temperature. Thus, the best effort we can take is to adopt the same procedure as in H14 to introduce an additional constraint on the dust temperature through radiative equilibrium argument. In this case,

the obtained upper limit for the dust mass is the same as in H14; therefore, we simply refer to H14 for the dust mass constraint in Model B.

In Fig. 4, we also show the expected ALMA sensitivities (the same as shown in Fig. 2, based on 5-h on-source integration with the full ALMA) at wavelengths 0.85, 1.2 and 2 mm (frequencies 350, 250 and 150 GHz). We observe that even with the full ALMA, this object is not detected unless $A_V > 0.05$ mag. If $A_V > 0.08$ mag, all the three bands can detect Himiko; in this case, we are able to give a strong constraint on the dust temperature and the total FIR luminosity (i.e. A_V). If the dust temperature is higher/lower under a fixed A_V, the detection at longer wavelengths becomes more/less difficult.

3.3 LBG sample

3.3.1 Fitting to the composite SED

We apply the same fitting procedure as above to the B16 LBG sample. Although each LBG would put only a much weaker constraint on the dust production than Himiko, the entire sample may give a strong constraint after stacking. Thus, we adopt the composite SED of the B16 LBGs constructed in Section 2.1 for the fitting. Since the age–extinction degeneracy is present, we apply Models A and B as two 'extremes' among the representative cases, following the fitting to Himiko. As mentioned above, the major difference between these two models is the contribution from the most recent ($\lesssim$10 Myr) star formation to the intrinsic UV slope. We regard Model A (continuous SFR) as more probable, since there is no reason that the LBG sample is biased to the objects without a recent ($\lesssim$10 Myr) star formation activity.

Because the ALMA upper limit flux relative to the UV flux is higher than that of Himiko, the constraint on the parameters is weaker (i.e. we find more solutions than in Himiko's case). The intrinsic (stellar) SED of Model A is bluer than the composite SED. Thus, we need a significant amount of extinction ($A_V \gtrsim 0.2$ mag). For the steepest extinction curve ($\delta = -1.1$), the upper bound of A_V is about 0.4 mag, which is determined by the rest UV SED; if A_V is larger than 0.4 mag, the rest UV SED is too red. If the extinction curve is flatter, we need a higher A_V, so that only high dust temperature is permitted to be consistent with the strong upper limit at 1.31 mm. Thus, there are two lines of solutions: (i) one is small $A_V \lesssim 0.4$ mag with a steep extinction curve and (ii) the other is large $A_V \gtrsim 0.7$ mag with a flat extinction curve and a high dust temperature. Since the composite SED reflects an averaged property for the extinction, we simply adopt a standard value for $\eta = 0.44$, appropriate for nearby starburst galaxies (Calzetti et al. 2000). We also examine the case of $\eta = 0$ later.

If we use reduced $\chi^2 < 3$ as a criterion of good fit following the case of Himiko, it also allows systematically redder SEDs that are not consistent with the flat wavelength dependence in the composite rest UV SED. We also found that the SED at $\lambda > 3$ μm does not constrain the parameters because the accepted flux ranges are wide. Thus, we only choose solutions that are within the shaded region at $\lambda < 3$ μm and below the 3σ upper limit at 1.3 mm in Fig. 1.

In Fig. 5, we show case (i) with $\delta = -1.1$. We show $A_V = 0.4$ mag with $T_d = 50$ K as an example of satisfactory fit. In the same figure, we also show case (ii) with $\delta = -0.4$, adopting $A_V = 0.7$ and 1 mag with the same dust temperature as above ($T_d = 50$ K). In case (ii), the rest UV SED is consistent with the composite SED even for $A_V = 1$; however, such a large A_V predicts large FIR luminosity, so that high dust temperature is required to be consistent with the ALMA upper limit. The rest UV SED ($\lambda < 3$ μm) is still as blue as seen in the composite SED because the extinction curve is flat. Since the total dust emission luminosity is higher than in case (i), the dust temperature should be $\gtrsim$50 K in case (ii) if A_V is as large as 1 mag. Therefore, the constraint on the dust temperature is tight for a flat extinction curve.

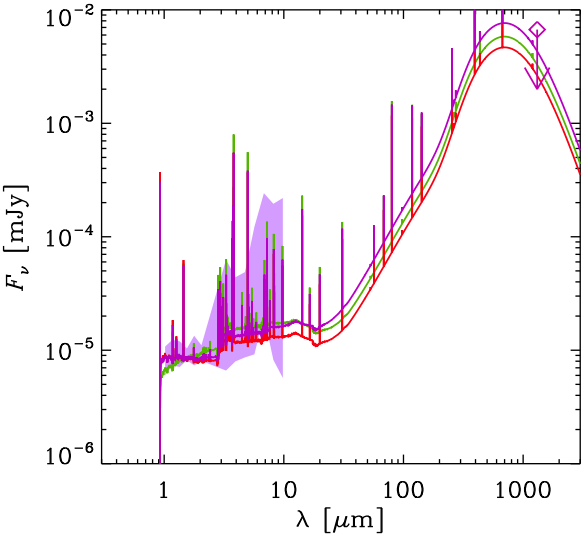

Figure 5. Examples of the fitting to the composite SED of the B16 LBG sample. Model A ($\tau_{SF} = 2000$ Myr and $t = 400$ Myr) is adopted with $\eta = 0.44$. The SEDs show the results with $(A_V\,[\mathrm{mag}], \delta) = (0.7, -0.4), (0.4, -1.1)$ and $(1, -0.4)$ for the lower to upper lines at mm wavelengths. The point with an arrow at 1.3 mm is a 3σ upper limit obtained by stacking, while the shaded region at $\lesssim$10 μm shows the probable area of the composite SED that is also shown in Fig. 1. Note that we only used the data at $\lambda < 3$ μm and the mm upper limit for the fitting (see the text).

We also confirmed that $\eta = 0$ gives the satisfactory fit to the UV SED as long as $A_V > 0.2$ mag (with $\delta = -1.1$; see also Section 3.3.2) in Model A. Therefore, the above assumption of $\eta = 0.44$ is not essential, but extinguishing the bluest stellar population with age <10 Myr is essential to reproduce the UV colour of the composite SED. It is not probable that the major part of the LBGs has stopped star formation in the last 10 Myr; thus, the dust extinction is the only probable way of systematically eliminating the contribution from the youngest (<10 Myr) population.

Nevertheless, we still investigate Model B ($\tau = 20$ Myr and $t = 200$ Myr), in which the population with age <10 Myr has negligible contribution to the intrinsic SED, because it is difficult to completely reject this model. For Model B, since the intrinsic stellar SED is already consistent with the observed SED, only $A_V < 0.1$ mag is permitted. With such a low extinction value, the FIR emission is well below the ALMA upper limit. However, as mentioned above, we regard Model B as improbable for the stacked data. Thus, we focus on Model A for the B16 sample.

3.3.2 Constraint on the dust mass

We estimate the dust mass for the allowed parameter ranges as already done for Himiko in Fig. 3 (Section 3.1). In Fig. 6, we show the dust mass on the (A_V, T_d) plane for $\delta = -1.1$ and -0.4 as representatives of steep (SMC-like) and flat extinction curves, respectively (Section 2.2). We adopt the same dust species (κ_ν) as adopted for Himiko in Section 3.1.

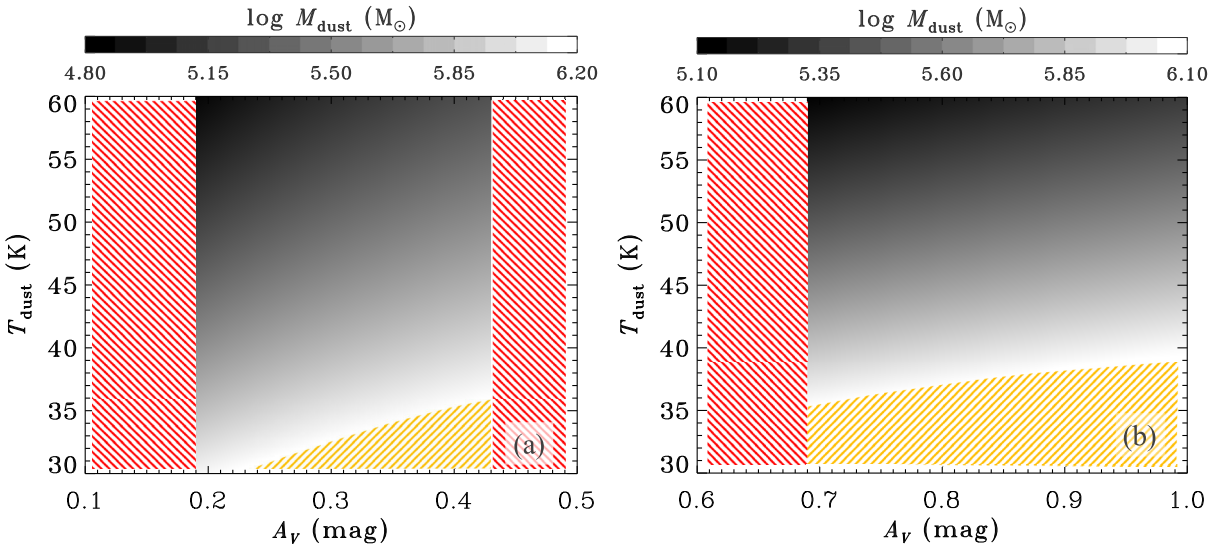

Figure 6. Same as Fig. 3 but for the dust mass obtained for the composite LBG SED. A steep extinction curve with $\delta = -1.1$ and a flat extinction curve with $\delta = -0.4$ are adopted for panels (a) and (b), respectively. For both panels, $\eta = 0.44$ is adopted.

We observe that 0.19 mag $< A_V <$ 0.43 mag is allowed for the steep extinction curve while 0.69 mag $< A_V$ is allowed for the flat extinction curve. The flat extinction curve requires a higher extinction to make the rest UV–optical SED as red as observed. Because the reddening is small, extinction as large as $A_V > 1$ mag is allowed in this case. Therefore, if a major part of LBGs have as flat an extinction curve as observed in high-z quasars, the extinction should be large, so that the correction for stellar mass and SFR for the extinction is as large as a factor of $\gtrsim$3 even at $z > 5$. If such a large fraction of star formation activity is enshrouded by dust, there should be a discrepancy between the time integration of the SFR traced in the UV and the observed stellar mass. However, there is no strong evidence of such discrepancy at $z > 5$ (Madau & Dickinson 2014). Therefore, we judge that the steep extinction curve with small $A_V \sim 0.2$–0.4 mag is more probable, although we should keep in mind that a flat extinction curve with large A_V could also give a consistent SED with observed LBGs at $z \gtrsim 5$. The dust temperature should be higher than 35 K for the flat extinction curve while dust temperatures as low as 30 K are allowed for the steep extinction curve. This is because large dust extinction for the flat extinction curve predicts a high dust emission luminosity, in which case the SED peak should be located at shorter wavelengths than 1.31 mm for the consistency with the ALMA upper limit. Overall, the constraint on the dust temperature is weaker compared with the case of Himiko, since the upper limit at the ALMA band relative to the UV continuum level is higher for the LBGs than for Himiko.

4 CONSTRAINT ON DUST PRODUCTION

H14 (see their section 3) proposed a method of constraining the dust production per SN. They basically divided the total dust mass by the number of SNe. The obtained dust mass per SN is an upper limit in the following two senses: (i) the estimate is based on an upper limit of the dust emission flux; and (ii) it is based on the assumption that all the dust is produced by SNe (i.e. it neglects other formation paths of dust). In this section, we briefly review their method and apply it to the dust masses obtained above for Himiko and LBGs.

4.1 Method of constraining SN dust production

We constrain the dust mass formed in a single SN by using the upper limit dust masses obtained above. If we assume that all the dust originates from dust condensation in SN ejecta, we can estimate the dust mass ejected from a single SN, $m_{\rm d,\,SN}$ as

$$m_{\rm d,SN} = \frac{M_{\rm d}}{(1 - f_{\rm dest}) N_{\rm SN}}, \tag{4}$$

where $f_{\rm dest}$ is the fraction of dust destroyed by SN shocks in the ISM, and $N_{\rm SN}$ is the total number of SNe (see also Michałowski 2015). We neglect the effect of dust recycling in star formation, since the assumption that SNe are the dominant source over grain growth indicates an early stage of chemical evolution (Dwek 1998; Zhukovska, Gail & Trieloff 2008; Inoue 2011). To obtain $m_{\rm d,\,SN}$, we need to estimate $N_{\rm SN}$ and $f_{\rm dest}$.

The total number of SNe at age t, $N_{\rm SN}(t)$, is estimated by

$$\begin{aligned} N_{\rm SN}(t) &= \int_0^t \int_{8\,{\rm M}_\odot}^{40\,{\rm M}_\odot} \psi(t' - \tau_m)\phi(m)\,{\rm d}m\,{\rm d}t' \\ &\simeq \int_0^t \psi(t')\,{\rm d}t' \int_{8\,{\rm M}_\odot}^{40\,{\rm M}_\odot} \phi(m)\,{\rm d}m, \end{aligned} \tag{5}$$

where $\psi(t)$ is the SFR at t, τ_m is the lifetime of a star with mass m (mass at the zero-age main sequence), $\phi(m)$ is the IMF and stars in the mass range of 8–40 $M_\odot$ are assumed to evolve into SNe (Heger et al. 2003). We assume that the lifetimes of SN progenitors are much shorter than t in order to simplify the first line of equation (5) to the second. For the consistency with the above SED fitting, we adopt the Chabrier IMF. The IMF is normalized so that the integral of $m\phi(m)$ for the entire mass range is 1.

The integration for the IMF in equation (5) indicates the number of SN progenitors per stellar mass, and is denoted as $\mathcal{F}_{\rm SN}$:

$$\mathcal{F}_{\rm SN} \equiv \int_{8\,{\rm M}_\odot}^{40\,{\rm M}_\odot} \phi(m)\,{\rm d}m. \tag{6}$$

We estimate that $\mathcal{F}_{\rm SN} = 9.9 \times 10^{-3}\,{\rm M}_\odot^{-1}$ for the IMF adopted. The other factor in equation (5) is the integrated SFR and is denoted

Table 2. Upper limits for the total dust mass (M_d) and dust mass produced per SN ($m_{d,SN}$).

Species[b]	Himiko Model A		Himiko Model B[a]		LBG Model A	
	M_d (10^6 $M_\odot$)	$m_{d,SN}$ ($M_\odot$)	M_d (10^6 $M_\odot$)	$m_{d,SN}$ ($M_\odot$)	M_d (10^6 $M_\odot$)	$m_{d,SN}$ ($M_\odot$)
Graphite	1.3	0.042	14	0.18	1.0	1.4
Silicate	2.1	0.067	20	0.25	1.6	2.3
SN_{con}	5.0	0.16	27	0.34	3.8	5.5
SN_{dest}	3.2	0.10	22	0.28	2.4	3.4
AC	0.97	0.031	8.9	0.11	0.74	1.0

Notes.[a]Because the dust temperature is not constrained in this model, the dust mass is not well determined. Thus, we put the dust mass constraint obtained using the radiative-equilibrium dust temperature derived by H14 (the total dust mass is the same as in their paper while the dust mass per SN is modified because we adopted a different IMF and stellar mass).
[b]See Table 1 and the text for the dust species.

as $\mathcal{M}_*$:

$$\mathcal{M}_* \equiv \int_0^t \psi(t')\,\mathrm{d}t'. \quad (7)$$

We are able to derive $\mathcal{M}_*$ from the SED fitting as an output quantity. Using the above two quantities, equation (5) is reduced to

$$N_{SN} = \mathcal{F}_{SN}\mathcal{M}_*. \quad (8)$$

H14 used a dust evolution model to estimate f_{dest}. The dust destruction is most prominently seen at the metallicity level where the dust growth by accretion starts to dominate the dust abundance. Thus, if we use the destroyed fraction at this metallicity level, we are able to obtain the most conservative (i.e. largest) value for f_{dest}. Following their estimate, we adopt $f_{dest} = 0.5$.

4.2 Constraint on SN dust for Himiko

In Section 3.1, we have shown that, if we adopt Model A (a continuous SFR) for Himiko, only high dust temperatures ($T_d > 70$ K) are allowed to make the dust emission SED consistent with the ALMA upper limit. Because of the high dust temperature as well as the tight ALMA upper limit, we obtain a stringent upper limit of 2.1×10^6 $M_\odot$ for the total dust mass (Section 3.1). H14 obtained an upper limit of 2.0×10^7 $M_\odot$ for the same dust material (silicate). The difference arises from their different method of estimating the dust temperature: H14 derived the dust mass based on the radiative equilibrium argument and obtained $T_d \sim 30$–40 K. As already discussed in Section 3.2, this dust temperature may be an underestimate because their estimate of the dust heating rate is based on the assumption that the dust is extended over the ALMA beam. Thus, the higher dust temperatures than obtained by H14 are not inconsistent with the current observational knowledge for Himiko.

Now we apply the method described in Section 4.1 to obtain a constraint on the dust mass per SN. We estimate the integrated SFR as $\mathcal{M}_* = 10^{9.8}$–$10^{9.9}$ $M_\odot$ for the SEDs with satisfactory fitting. Thus, using equation (8), we obtain the total number of SNe as $N_{SN} = (6.2$–$7.9) \times 10^7$. Using equation (4) and recalling that $f_{dest} = 0.5$, we finally obtain $m_{d,SN} < 0.053$–0.067 $M_\odot$ based on the upper limit of M_d (2.1×10^6 $M_\odot$). We take the larger value as a conservative limit (0.067 $M_\odot$). The dust masses obtained for other dust species are listed in Table 2.

For Model B, because the dust temperature is not constrained by our method, we simply adopt the dust mass obtained by H14 as mentioned in Section 3.2. The integrated stellar mass is $\mathcal{M}_* = 10^{10.2}$–$10^{10.3}$ $M_\odot$ in Model B of Himiko. This leads to the number of SNe as $N_{SN} = (1.6$–$1.8) \times 10^8$. Using equation (4) together with $f_{dest} = 0.5$, we obtain $m_{d,SN} < 0.22$–0.25 $M_\odot$ for silicate based on the upper limit of M_d (2.0×10^7 $M_\odot$). We take the larger value as a conservative limit (0.25 $M_\odot$). The upper limit obtained for each dust species is listed in Table 2.

4.3 Constraint on SN dust for LBGs

We apply the same method as above to constrain the dust mass produced per SN for the LBG sample in B16. Because Model B does not put a meaningful constraint on M_d (Section 3.3.1), we concentrate on Model A. In Section 3.3, we used the composite SED to constrain the total dust mass, obtaining an upper limit of $\sim 1.6 \times 10^6$ $M_\odot$ (we adopt $\delta = -1.1$, since this gives a more conservative upper limit than $\delta = -0.4$) for silicate. In Table 2, we list the corresponding upper limits for the different species. For the composite SED, we obtain the integrated SFR as $\mathcal{M}_* = 1.4 \times 10^8$ $M_\odot$. Thus, from equation (8), we obtain $N_{SN} = 1.4 \times 10^6$. Using equation (4) along with $f_{dest} = 0.5$, we finally obtain an upper limit of $m_{d,SN} < 2.3$ $M_\odot$. The dust mass obtained for other dust species are listed in Table 2.

The upper limit of $m_{d,SN}$ obtained for the LBGs is too large to put a useful constraint on the SN dust production theory. This weaker constraint than in the case of Himiko arises from the much smaller number of SNe (N_{SN}). Therefore, in order to obtain a strong constraint on $m_{d,SN}$, it is desirable to observe a system in which a large number of SNe have occurred. Because the number of SNe is proportional to the total stellar mass (with a fixed IMF), observations of objects with high (stellar) UV luminosity give strong constraint on $m_{d,SN}$.

5 DISCUSSION

We have shown that we are able to put a strong constraint on the dust mass in Himiko. There are two ways of reproducing the observed rest-UV colour: one is to apply a blue SED with significant dust extinction for the youngest ($\lesssim$10 Myr) stellar population, and the other is to assume a stellar population that lacks the youngest population. The first and second cases correspond to Models A and B, respectively. The derived dust mass depends on which model to adopt. Although we are not able to draw a definite conclusion regarding which model is correct for Himiko or LBGs, we here mainly discuss how we will be able to distinguish between the two models.

5.1 How to distinguish between Models A and B

The largest difference between Models A and B is the magnitude of dust extinction. Model A, which requires more extinction than Model B, tends to predict higher total dust luminosities; thus, for the consistency with the ALMA upper limits, higher dust temperatures are required in Model A than in Model B. For Himiko, we obtained dust temperatures higher than 70 K in Model A. With such a high temperature, the SED peak is located at a shorter wavelength than the ALMA 1.2 mm band. Therefore, if we observe Himiko at a shorter wavelength such as at 850 μm, we could see if the high dust temperature is really the solution as we already discussed in Section 3.

For the stacked SED of the B16 LBG sample, dust temperatures as low as ∼40 K are still allowed (Fig. 6). The weak constraint is due to the faint UV flux. Because the UV flux of an LBG is on average 30–50 times lower than that of Himiko, we need $\sim 30^2$–50^2 LBGs to obtain as strong constraint as we obtained for Himiko. In order words, the observation of an object whose UV flux is as bright as Himiko is 1000–3000 times more powerful in terms of the integration time than that of a normal LBG in constraining the SN dust production.

5.2 High dust temperature

In the above, we suggested a high dust temperature for Himiko. Indeed, some studies have suggested that the dust temperatures in high-z star-forming galaxies are high. Ouchi et al. (1999) showed that dust temperatures should be higher than 40 K for $z \sim 3$ LBGs if the lack of detection by SCUBA is taken into account. B16 derived similarly high dust temperatures for LBGs at $z \gtrsim 5$ based on the deficit of ALMA detection.

There are also some theoretical studies that suggested high temperatures in high-z galaxies. Ferrara et al. (2017) estimated that the dust temperature in LBGs could be as high as $\gtrsim$50 K if the spatial distribution of dust is as compact as the stellar distribution. Narayanan et al. (2017), using their cosmological hydrodynamic simulation and radiation transfer calculation, showed that the dust temperatures in high-z dusty star-forming galaxies are as high as 50–70 K. These studies give a physical reason for the high dust temperatures at high z.

There are some LBGs at $z > 5$ whose dust continuum was detected by ALMA (Capak et al. 2015; Watson et al. 2015; Laporte et al. 2017). Although we need careful one-by-one analysis for those galaxies, our preliminary results (Burgarella et al., in preparation) indicate that they tend to have high dust temperatures (see Faisst et al. 2017, for a very recent result). In future more sensitive observations by the full ALMA will also serve to detect more high-z LBGs at multiple submm–mm wavelengths, enabling us to determine the dust temperatures. This leads to solving the degeneracy between age and dust extinction.

5.3 Constraint on the SN dust production

In Section 4.1, we constrained the dust mass produced per SN. We obtained a strong upper limit as $m_{\rm d,\,SN} \lesssim 0.1$ M$_\odot$ for Himiko if we adopt Model A. If we recall the discussion in Section 4.1, the constraint on $m_{\rm d,\,SN}$ was obtained from the dust mass divided by the number of SNe. The number of SNe was derived from the time integration of SFR. Although the age and the SFR are uncertain in the SED fitting, the estimate of integrated SFR is robust since it is determined by the observed stellar continuum level. Therefore, the smallness of $m_{\rm d,\,SN}$ is a robust conclusion derived from the ALMA upper limit and the rest-UV flux.

The small $m_{\rm d,\,SN}$ indicates either that reverse shock destruction in SNe is efficient because of high ambient medium density ($\gtrsim$10 cm^{-3}; Bianchi & Schneider 2007; Nozawa et al. 2007), or that the dust is lost for some reason such as galactic winds, etc. The possibility of high ambient density may be supported by Pallottini et al. (2017), who showed based on their hydrodynamic simulation that the central gas disc of a high-z galaxy has a density higher than 25 cm^{-3}. In such a dense environment, reverse shock destruction could be efficient. For the latter possibility, Hou et al. (2017), based on the numerical simulation developed by Aoyama et al. (2017), showed that dust can be transported into the circumgalactic space by SN feedback. Bekki, Hirashita & Tsujimoto (2015) suggested that the dust loss by stellar feedback could be important in explaining the extinction curve in the SMC.

The above scenario of low $m_{\rm d,\,SN}$ implies that the dust enrichment by SNe is not efficient at high z. Probably other mechanisms such as dust production by AGB stars (Valiante et al. 2009) and dust growth in the dense ISM (Mancini et al. 2015; Popping, Somerville & Galametz 2017; Wang et al. 2017) are necessary to produce an appreciable amount of dust at high z (see also Ferrara, Viti & Ceccarelli 2016; Zhukovska et al. 2016). We note that, even if we consider other processes of dust formation, the values of $m_{\rm d,\,SN}$ obtained above are still an upper limit because we assumed that all dust is produced by SNe.

6 CONCLUSION

We investigate the possibility of constraining the dust mass in high-z ($z \gtrsim 6$) galaxies by applying SED fitting (CIGALE) to rest UV–optical photometric data and the ALMA upper limits. For SED fitting, there is a well-known degeneracy between dust extinction and stellar age. Moreover, the Lyα emission line is not necessarily associated with star formation activity, which means that the bright Lyα emission cannot completely exclude a possibility of old stellar age. Therefore, we focus on two extremes for the star formation history: one is continuous star formation that includes very young ($<$10 Myr) population (Model A), and the other is instantaneous star formation in which the SFR has declined (with negligible young stellar population with ages $<$10 Myr; Model B). These models are applied to Himiko and the B16 LBG sample.

For Himiko, Model A predicts significant dust extinction to explain the observed rest-UV SED. The predicted 1.2 mm flux is consistent with the strong ALMA upper limit only if the dust temperature is higher than 70 K. Because of the high dust temperature (i.e. high emission efficiency), we obtain a strong upper limit for the dust mass $\sim 2 \times 10^6$ M$_\odot$. Based on this value, the dust mass produced per SN is estimated as $\lesssim$0.1 M$_\odot$. This low value indicates that dust once condensed is destroyed in the shocked region associated with the SN, or that dust is lost out of the main body of the galaxy. If this is true for other galaxies at high z, SNe may not be the main source of dust there, and we need to consider other processes for dust enrichment such as dust growth in the dense ISM. In contrast, Model B allows an order of magnitude larger dust mass $\sim 2 \times 10^7$ M$_\odot$, which is converted to the dust mass produced by an SN as ∼0.3 M$_\odot$. We could distinguish between Models A and B if we observe Himiko at a shorter wavelength than 1.2 mm by the full ALMA. The high dust temperatures in Model A predict that Himiko can be detected at 0.85 mm.

For the LBG sample in B16, we make a composite SED to put a strong constraint on the ALMA mm flux. The composite SED

indicates that the dust mass is $\sim 2 \times 10^6$ $M_\odot$ or less in a typical LBG at $z > 5$, but this only puts a weak upper limit for the dust mass produced per SN as $\lesssim 2$ $M_\odot$. We estimate that, in order to obtain an upper limit comparable to Himiko for SN dust production, we need to observe 1000–3000 LBGs. This clarifies the importance of observing UV-bright objects (like Himiko) to constrain the dust production by SNe.

ACKNOWLEDGEMENTS

We are grateful to the anonymous referee for useful comments. HH thanks the staff at LAM for their hospitality and financial and technical support during my stay. HH is supported by the Ministry of Science and Technology grant MOST 105-2112-M-001-027-MY3.

REFERENCES

Aoyama S., Hou K.-C., Shimizu I., Hirashita H., Todoroki K., Choi J.-H., Nagamine K., 2017, MNRAS, 466, 105
Aravena M. et al., 2016, ApJ, 833, 71
Asano R. S., Takeuchi T. T., Hirashita H., Nozawa T., 2014, MNRAS, 440, 134
Baes M., Verstappen J., De Looze I., Fritz J., Saftly W., Vidal Pérez E., Stalevski M., Valcke S., 2011, ApJS, 196, 22
Bekki K., Hirashita H., Tsujimoto T., 2015, ApJ, 810, 39
Bianchi S., 2008, A&A, 490, 461
Bianchi S., Schneider R., 2007, MNRAS, 378, 973
Bouwens R. J. et al., 2014, ApJ, 793, 115
Bouwens R. J. et al., 2016, ApJ, 833, 72
Bruzual G., Charlot S., 2003, MNRAS, 344, 1000
Buat V., Burgarella D., 1998, A&A, 334, 772
Buat V., Xu C., 1996, A&A, 306, 61
Buat V. et al., 2012, A&A, 545, A141
Burgarella D., Buat V., Iglesias-Páramo J., 2005, MNRAS, 360, 1413
Calzetti D., 2001, PASP, 113, 1449
Calzetti D., Kinney A. L., Storchi-Bergmann T., 1994, ApJ, 429, 582
Calzetti D., Armus L., Bohlin R. C., Kinney A. L., Koornneef J., Storchi-Bergmann T., 2000, ApJ, 533, 682
Capak P. L. et al., 2015, Nature, 522, 455
Carroll S. M., Press W. H., Turner E. L., 1992, ARA&A, 30, 499
Casey C. M., 2012, MNRAS, 425, 3094
Cazaux S., Tielens A. G. G. M., 2004, ApJ, 604, 222
Chabrier G., 2003, PASP, 115, 763
Charlot S., Fall S. M., 2000, ApJ, 539, 718
Conroy C., 2013, ARA&A, 51, 393
da Cunha E., Charlot S., Elbaz D., 2008, MNRAS, 388, 1595
Dayal P., Hirashita H., Ferrara A., 2010, MNRAS, 403, 620
De Looze I. et al., 2014, A&A, 571, A69
Draine B. T., Lee H. M., 1984, ApJ, 285, 89
Dwek E., 1998, ApJ, 501, 643
Faisst A. L. et al., 2017, ApJ, in press (arXiv:1708.07842)
Ferrara A., Viti S., Ceccarelli C., 2016, MNRAS, 463, L112
Ferrara A., Hirashita H., Ouchi M., Fujimoto S., 2017, MNRAS, 471, 5018
Fudamoto Y. et al., 2017, MNRAS, 472, 483
Gallerani S. et al., 2010, A&A, 523, A85
Gould R. J., Salpeter E. E., 1963, ApJ, 138, 393
Heger A., Fryer C. L., Woosley S. E., Langer N., Hartmann D. H., 2003, ApJ, 591, 288
Hirashita H., Ferrara A., 2002, MNRAS, 337, 921
Hirashita H., Nozawa T., Kozasa T., Ishii T. T., Takeuchi T. T., 2005, MNRAS, 357, 1077
Hirashita H., Nozawa T., Takeuchi T. T., Kozasa T., 2008, MNRAS, 384, 1725
Hirashita H., Ferrara A., Dayal P., Ouchi M., 2014, MNRAS, 443, 1704
Hou K.-C., Hirashita H., Michałowski M. J., 2016, PASJ, 68, 94
Hou K.-C., Hirashita H., Nagamine K., Aoyama S., Shimizu I., 2017, MNRAS, 469, 870
Inoue A. K., 2005, MNRAS, 359, 171
Inoue A. K., 2011, Earth Planets Space, 63, 1027
Kennicutt R. C., Evans N. J., 2012, ARA&A, 50, 531
Laporte N. et al., 2017, ApJ, 837, L21
Madau P., Dickinson M., 2014, ARA&A, 52, 415
Maiolino R., Schneider R., Oliva E., Bianchi S., Ferrara A., Mannucci F., Pedani M., Roca Sogorb M., 2004, Nature, 431, 533
Mancini M., Schneider R., Graziani L., Valiante R., Dayal P., Maio U., Ciardi B., Hunt L. K., 2015, MNRAS, 451, L70
Mancini M., Schneider R., Graziani L., Valiante R., Dayal P., Maio U., Ciardi B., 2016, MNRAS, 462, 3130
Maraston C., 2005, MNRAS, 362, 799
Matsuura M. et al., 2011, Science, 333, 1258
Meurer G. R., Heckman T. M., Calzetti D., 1999, ApJ, 521, 64
Michałowski M. J., 2015, A&A, 577, A80
Narayanan D., Dave R., Johnson B., Thompson R., Conroy C., Geach J. E., 2017, MNRAS, submitted (arXiv:1705.05858)
Noll S., Burgarella D., Giovannoli E., Buat V., Marcillac D., Muñoz-Mateos J. C., 2009, A&A, 507, 1793
Nozawa T., Kozasa T., Umeda H., Maeda K., Nomoto K., 2003, ApJ, 598, 785
Nozawa T., Kozasa T., Habe A., Dwek E., Umeda H., Tominaga N., Maeda K., Nomoto K., 2007, ApJ, 666, 955
Nozawa T., Asano R. S., Hirashita H., Takeuchi T. T., 2015, MNRAS, 447, L16
Omukai K., Tsuribe T., Schneider R., Ferrara A., 2005, ApJ, 626, 627
Ouchi M., Yamada T., Kawai H., Ohta K., 1999, ApJ, 517, L19
Ouchi M. et al., 2009, ApJ, 696, 1164
Ouchi M. et al., 2013, ApJ, 778, 102
Pallottini A., Ferrara A., Gallerani S., Vallini L., Maiolino R., Salvadori S., 2017, MNRAS, 465, 2540
Pei Y. C., 1992, ApJ, 395, 130
Popescu C. C., Tuffs R. J., Dopita M. A., Fischera J., Kylafis N. D., Madore B. F., 2011, A&A, 527, A109
Popping G., Puglisi A., Norman C. A., 2017, MNRAS, in press (arXiv:1706.06587)
Popping G., Somerville R. S., Galametz M., 2017, MNRAS, 471, 3152
Salpeter E. E., 1955, ApJ, 121, 161
Schneider R., Omukai K., Inoue A. K., Ferrara A., 2006, MNRAS, 369, 1437
Silva L., Granato G. L., Bressan A., Danese L., 1998, ApJ, 509, 103
Takagi T., Arimoto N., Vansevičius V., 1999, ApJ, 523, 107
Takagi T., Vansevicius V., Arimoto N., 2003, PASJ, 55, 385
Takeuchi T. T., Ishii T. T., Nozawa T., Kozasa T., Hirashita H., 2005, MNRAS, 362, 592
Takeuchi T. T., Yuan F.-T., Ikeyama A., Murata K. L., Inoue A. K., 2012, ApJ, 755, 144
Todini P., Ferrara A., 2001, MNRAS, 325, 726
Valiante R., Schneider R., Bianchi S., Andersen A. C., 2009, MNRAS, 397, 1661
Wang W.-C., Hirashita H., Hou K.-C., 2017, MNRAS, 465, 3475
Watson D., Christensen L., Knudsen K. K., Richard J., Gallazzi A., Michałowski M. J., 2015, Nature, 519, 327
Willott C. J., Carilli C. L., Wagg J., Wang R., 2015, ApJ, 807, 180
Yajima H., Nagamine K., Thompson R., Choi J.-H., 2014, MNRAS, 439, 3073
Yamasawa D., Habe A., Kozasa T., Nozawa T., Hirashita H., Umeda H., Nomoto K., 2011, ApJ, 735, 44
Zhukovska S., Gail H.-P., Trieloff M., 2008, A&A, 479, 453
Zhukovska S., Dobbs C., Jenkins E. B., Klessen R. S., 2016, ApJ, 831, 147
Zubko V. G., Mennella V., Colangeli L., Bussoletti E., 1996, MNRAS, 282, 1321
Zubko V., Dwek E., Arendt R. G., 2004, ApJS, 152, 211

This paper has been typeset from a TEX/LATEX file prepared by the author.